Patient-specific voxel phantom dosimetry during the prostate treatment with high-energy linac

Najmeh Mohammadi · Hashem Miri-Hakimabad ·
Laleh Rafat-Motavalli · Fatemeh Akbari ·
Sara Abdollahi

Abstract Dose due to neutrons resulting from high-energy linear accelerator is not detailed in routine treatment planning, though this information is potentially important for better estimates of health risks including secondary cancers. In this study, the neutron contaminations were evaluated in the patient-specific voxel phantom for the treatment of prostate cancer using MCNP code. The results showed that the neutron organ doses are independent from the distance between studied organs and treatment area, and unlike the photon dose, the neutron dose distribution is almost homogeneous in the patient body.

Keywords Voxel phantom · Dosimetry · High-energy linacs · Monte Carlo

Introduction

Nowadays, the prostate cancer is one of the most frequent types of cancers in men. The radiotherapy with high-energy medical linear accelerators (LINACS) is used most often for treating this cancer. However, unwanted doses from secondary neutrons produced in the linac operating above the 8 MV, increase the risk of secondary cancer in the patients [1–3]. These neutrons are produced through the photonuclear interactions with high-Z materials of the linac's head [4, 5]. Then, they deposit their energies while they are passing through the jaws, and the shield around the head or scattering from the walls and floor of the treatment room. The energy spectra of these neutrons have peaks between 0.1 and 1 MeV [6], which have the maximum radiation weighting factor [7]. Thus, these neutron energies are very effective in damaging tissues [8].

Despite the importance of the deposited energy of neutrons in the patient body, they are not considered in the routine treatment planning [9]. As known, the doses delivered to the patient body cannot be measured directly. Therefore, some computer codes such as MCNP were developed to determine the unwanted neutron doses.

For this purpose, some authors calculated the neutron contamination in the mathematical anthropomorphic phantom [10]. Recently, Thalhofer et al. [11] and Martinez-Ovalle et al. [12] used the voxel MAX phantom for calculating doses delivered to the patients undergoing a pelvic treatment with an accelerator operating at 18 MV.

Specifically, this paper is devoted to study neutron dose calculations in the organs of a patient-specific voxel phantom undergoing the prostate treatment with a 15 MV Primus Siemens accelerator, using MCNPX2.6 [13].

Materials and methods

Patient-specific phantom

Since the dose received by the patient's organs depends on the various parameters such as weight, size, and the location of organs, it is preferred to construct patient-specific voxel phantom for dose estimations.

For this purpose, a total number of 53 CT images with resolution of 512×512 and slice thickness of 0.5 cm from the pelvis area of a cancer patient were used. Using

N. Mohammadi · H. Miri-Hakimabad (✉) · L. Rafat-Motavalli
Faculty of Sciences, Ferdowsi University of Mashhad, Mashhad,
Iran
e-mail: mirihakim@yahoo.com; mirihakim@um.ac.ir

F. Akbari · S. Abdollahi
Reza Radiation Oncology Center, Mashhad, Iran

software 3D-DOCTOR^{TM} software (Able Software Corp., Lexington, MA) organs and tissues including the large intestine, small intestine, pelvis bone (including cortical and spongiosa), lymph nodes, skin, prostate, urinary bladder, rectum, muscle, femur (including cortical and spongiosa), and spine were segmented. 3D-DOCTOR provides a polygon mesh model for each image set. Each polygon mesh model was exported as a Wavefront Object file, a format that is easily imported into most 3D modeling software packages.

Considering that in the treatment planning CT images are taken from the treatment area, the CT images of total body of the patient were not available. On the other hand, a completed model of patient was needed to estimate the neutron contamination in the whole body. Therefore, the ICRP male reference phantom was selected as template, which is recommended for dosimetry calculation of a human body [14]. Then to develop the full model of patient body, the organs/tissues located in the abdominal and pelvis regions of the patient were inserted in the reference phantom. For this end, the polygon mesh 'Wavefront Object' files of the ICRP male reference phantom and segmented organs of patient were imported into 'Rhinoceros^{TM}' (McNeel North America, Seattle, WA), a NURBS and polygon mesh modeling software package. Organs of the abdominal and pelvic region of the base phantom (ICRP male reference) were replaced with those of the patient. This process is similar to what used by Hoseinian-Azghadi et al. [15].

Finally, the voxelization process of the hybrid phantom was done using an innovative method developed by our research group. The resulting voxel resolution was 2.137 mm × 2.137 mm × 8 mm. Then the composition materials and their densities were assigned to each voxel, based on ICRP male reference phantom. The schematic representation of 3D-model of segmented organs of patient and final voxel phantom are shown in the Fig. 1.

Simulation of treatment plan

The detailed geometry of the head of 15 MV Primus Siemens was simulated using MCNPX2.6. The simulated model was validated in the previous study [16]. The simulated prostate treatment plan was based on the RtDosePlan software [17] for treatment planning system at the Reza Radiation Oncology Center (RROC) with four-filed box plan. The irradiation fields in the treatment planning system (TPS) were 16×20.6 cm^2 for anterior–posterior (AP), and posterior–anterior (PA), with monitor units (MUs) of 51, 48, respectively, while they were 10×20.6 cm^2 for left-lateral (LLAT), and right-lateral (RLAT) irradiations with MUs of 63. In all irradiation fields, the prostate was placed at the isocenter. The goal of TPS was delivering 200 cGy to the gross tumor volume

(GTV), which is prostate, during the irradiation time in each fraction. In the radiotherapy of pelvis area, the patient's hands are usually placed in the front of the head, so in the simulations, the phantom arms were eliminated.

Monte Carlo simulation

The MCNPX code version 2.6 was used to transport electrons, photons, and neutrons. Using PHY card, the photoneutron productions were considered. The energy cutoff for electrons and photons were assumed 0.5 and 0.01 MeV, respectively. To save time, the particles were recorded in the surface above the jaws (phase space) using the ssw card. Then for following calculations, these data were read using the ssr card. A total of 2×10^9 initial electrons were transported and 7×10^8 particles (included electrons, photons, and neutrons) were scored in the phase space. For neutron calculations, the energy cutoff of electrons and photons was set 7 MeV, below the threshold of photonuclear interactions. To determine the isodose curves, the mesh tally (type 3) was used, and the energy deposited in each voxel (MeV/cm^3) was divided by the voxel density and was multiplied by 160 to achieve the absorbed dose in terms of pGy. The relative errors in the photon calculations were less than 3 %. Then the following formula was used for calculating dose value in terms of cGy in each voxel;

$$D = \sum_k D_{\text{MC}} \times \text{MU}(k)/D_{\text{calibration point}} \qquad (1)$$

where the summation is on the gantry angle (that is AP, PA, LLAT, and RLAT), D_{MC} is the photon absorbed dose in each voxel (in term of pGy), and the $D_{\text{calibration point}}$ is dose of calibration point (in term of pGy) corresponds to depth of d_{max} in 10×10 cm^2 irradiation field, in which 1 MU = 1 cGy.

The absorbed dose from photons and neutrons to all organs and tissues were calculated using the track-length energy deposition tally (F6). In photon calculations, this tally provides the collision kerma averaged throughout the organ. Therefore, we assumed that in the organs and tissues, the conditions of electronic equilibrium are satisfied and the dose and kerma are nearly the same. To test this assumption, we compared absorbed dose and kerma in several organs for a selected number of fields. The results confirmed that this assumption holds for the treatment plans considered in this work.

Protection quantities: equivalent dose and effective dose

According to ICRP 103 [7], the protection quantities are the equivalent dose in organs or tissues and the effective dose. The equivalent dose of tissue T (H_T) is defined as:
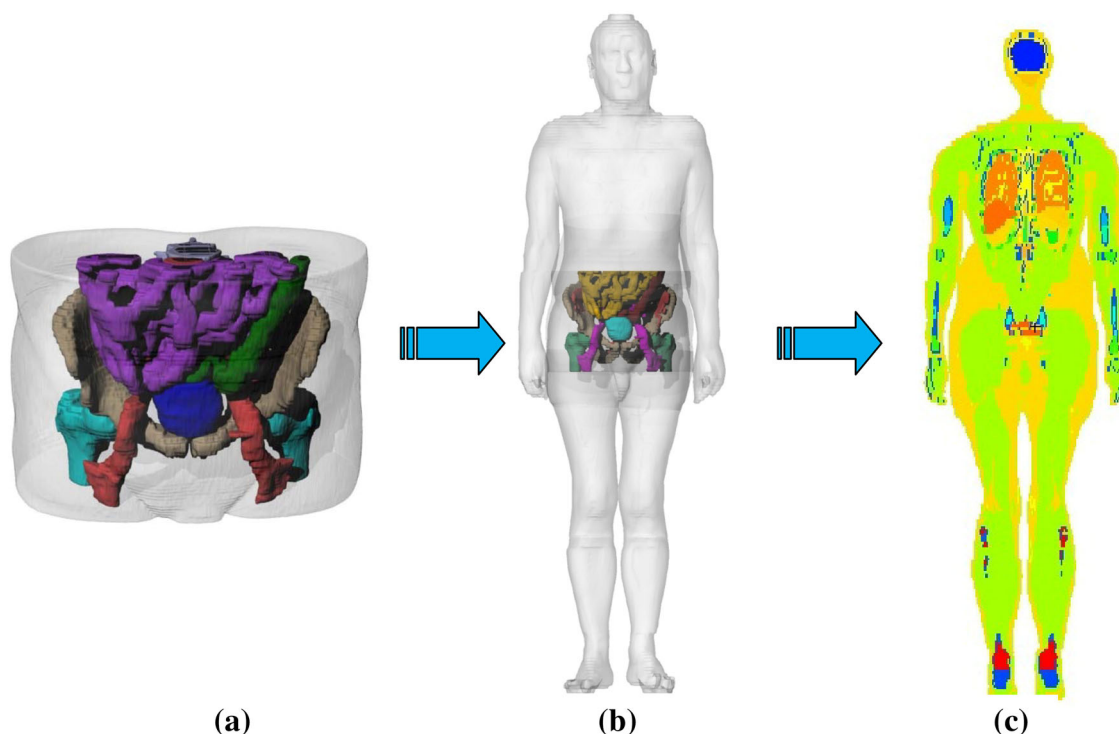
Fig. 1 a 3D-model of segmented organs, **b** replacing the 3D-model of patient organs in the ICRP phantom, **c** final patient-specific voxel phantom

$$H_T = \sum_R W_R \times D_{T,R} \tag{2}$$

where $D_{T,R}$ is the average absorbed dose due to radiation of type R in the volume of a specific organ or tissue, and W_R is the radiation weighting factor for radiation type R. For photons, W_R is equal to 1 and organ absorbed dose is the same as equivalent dose. However, neutrons' W_R is depending on the neutron incident energy. Therefore, the weighted W_R averaged above the phantom surface was calculated and it was found that $\overline{W_R} = 15.3$. Another protection quantity defined by ICRP 103 is effective dose E, which is used to estimate the received dose by whole body:

$$E = \sum_T W_T \times H_T \tag{3}$$

where W_T is the weighting factor for organ or tissue T, and H_T is the equivalent dose of tissue T.

Risk of developing a fatal secondary malignancy

Once the organ equivalent doses were estimated, the secondary cancer risk was calculated using the probability coefficients of National Council of Radiation Protection and Measurements (NCRP) in the Report 116 [18]. The most commonly used risk coefficients are those compiled by this report, shown in Table 1. These risk coefficients,

representing the absolute lifetime risk of developing a fatal secondary malignancy weighted over all age groups, were based predominantly on data from Japanese atomic bomb survivors. These coefficients refer to bladder, bone marrow, bone surface, breast, colon, liver, lung, esophagus, gonads, skin, stomach, thyroid, and remainder. In this

Table 1 Lifetime probabilities of developing fatal secondary malignancies by organ site

Organ	Probability of fatal cancer (%/Sv)
Bladder	0.30
Bone marrow	0.50
Bone surface	0.05
Breast	0.20
Esophagus	0.30
Colon	0.85
Liver	0.15
Lung	0.85
Gonads	0.10
Skin	0.02
Stomach	1.10
Thyroid	0.08
Remainder of body	0.50
Total	5.00

study, spleen, pancreas, kidneys, prostate, brain, adrenals, intestine wall, thymus, and rectum were assumed as remainder organs.

Results and discussion

### Comparison between Monte Carlo and TPS

The calculated isodose curves with Monte Carlo (MC) and TPS in the transverse plan are shown in the Fig. 2. It was observed that the both dose distributions follow a very similar pattern. There were good agreements between the results of calculation and TPS. Therefore, it could be concluded that the simulation of treatment plan and patient-body were well implemented using Monte Carlo. The cumulative dose volume histogram (DVH) of photons in the prostate, bladder, and rectum are illustrated in the Fig. 3. As seen, the entire prostate and rectum volumes were covered by 100 % of the prescribed dose of 200 cGy in TPS. While the Monte Carlo method showed that only about 90 % of the prescribed dose was delivered to the target volume and rectum. Because the whole volume of

urinary bladder was not in the irradiation field, its DVH had different behavior. The total volume urinary bladder was covered by 113 cGy in TPS, while this value was 103 cGy in the Monte Carlo calculation. Thus, with these coincidences the Mont Carlo calculations are reliable and can be employed for photon and neutron dosimetry.

Equivalent dose of photons

The photon equivalent doses of different organs and tissues per 1 Gy prostate absorbed dose for each gantry angle are listed in the Table 2. Photon equivalent dose varied in the large range from 1,015.66 to 2.18 mSv/Gy for organs located in the treatment area and healthy organs located far from it, respectively. As expected, the higher photon dose was stored in the organs close to treatment area, and as organ distance from the treatment area increased the amount of photon absorbed dose reduced. From the results, rectum was the organs that received the maximum equivalent dose of 1,015.66 mSv/Gy. After that the sacrum, urinary bladder, and pelvis received higher photon doses of 941.89, 798.48, and 750.39 mSv/Gy, respectively. From Table 2, thymus, which was the normal tissue and located

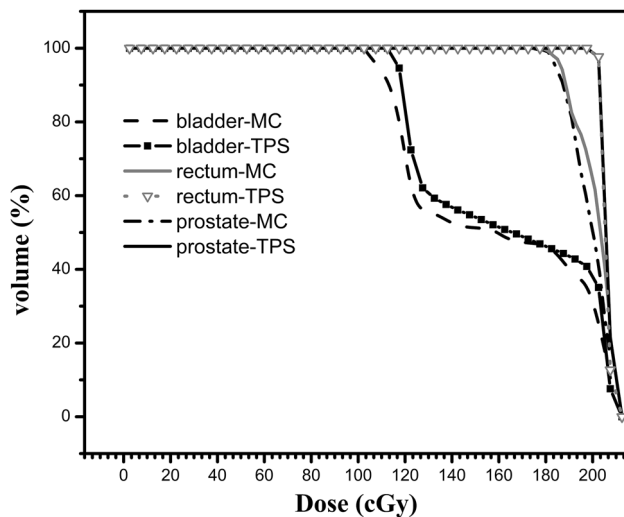**Fig. 2** Isodose curves calculated by **a** TPS and **b** MC
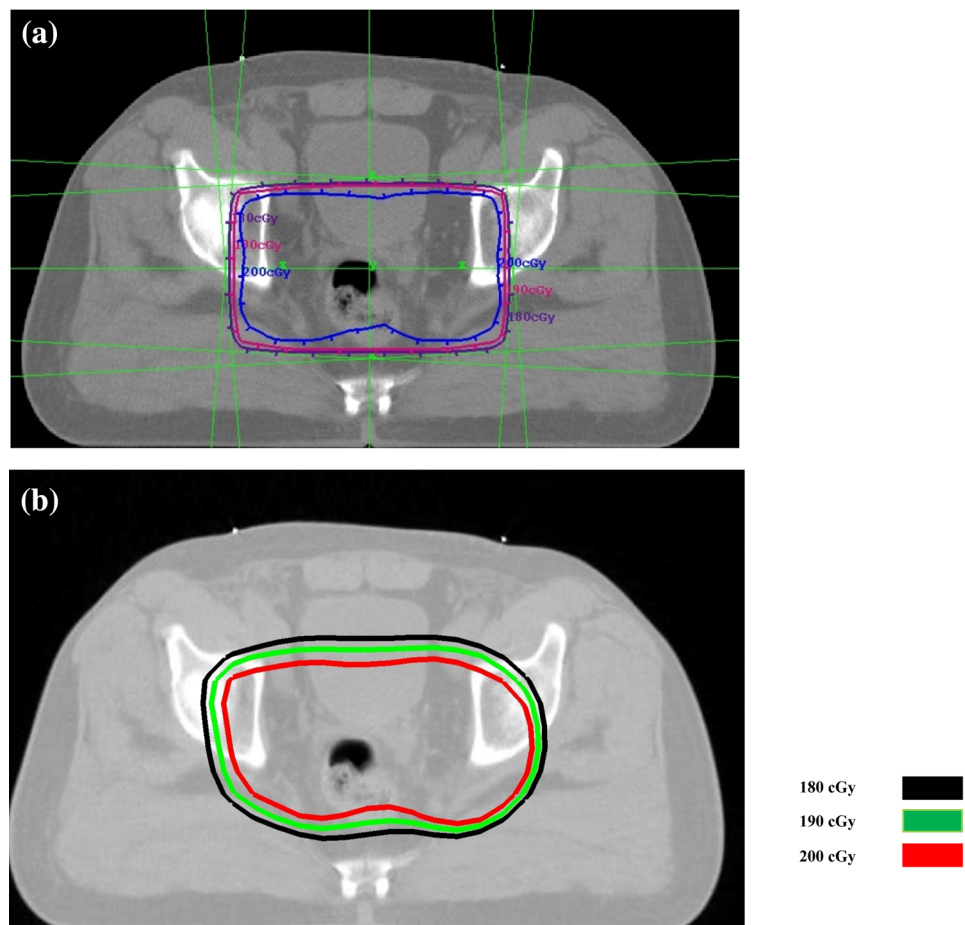
Fig. 3 DVH curves determined by MC and TPS for urinary bladder, rectum, and prostate

out of the irradiation field, received the minimum value of photon equivalent dose of 2.18 mSv/Gy. The deposited dose of photon in the organs depended on the gantry orientation, because in each orientation incident photons passed through different tissues. For instance, in the AP irradiation, urinary bladder, thyroid, thymus, and esophagus received greater share of dose. This photon dose distribution validated the goal of radiotherapy, which is delivering the maximum dose to the treatment area.

Equivalent dose of neutrons

The neutron equivalent doses per 1 Gy prostate photon absorbed dose together with their relative statistical uncertainties are provided in the Table 3. From the results, uncertainties in some organs/tissues were larger than 10 %. As Martinez-Ovalle et al. concluded, the neutron equivalent dose was reduced strongly by increasing the depth. This reduction is closely related to the cross section of elastic scattering of neutron with hydrogen at the maximum energies presented in the neutron spectra [19]. Thus, the results, which had the uncertainties less than 10 %, would be discussed. According to the obtained results, residual tissues (adipose tissue under the skin, and soft tissue located between the organs), ankles and foot bones, salivary glands, muscle, and testes received the higher values of neutron equivalent doses of 0.34, 0.29, 0.29, 0.23, and 0.23 mSv/Gy, respectively. Tibiae–fibulae–patellae, urinary bladder, and colon were also received significant amount of equivalent neutron doses of 0.2, 0.21, and 0.19 mSv/Gy, respectively.

From the obtained results, the neutron dose varied according to the gantry angle. For example, the lymphatic

Table 2 Photon equivalent dose calculated for different organs/tissues (mSv/Gy)

Organ/tissue	AP	PA	RLAT	LLAT	Total
Rectum	924.45	1,097.07	1,044.92	1,013.97	1,015.66
Sacrum	882.32	1,113.48	873.69	910.42	941.89
Urinary bladder	1,204.62	858.51	531.80	532.92	798.48
Pelvis	592.23	641.15	877.64	913.34	750.39
Lymphatic nodes	650.62	522.47	426.51	431.47	513.44
Femora	55.14	60.40	364.19	375.69	208.38
Small intestine	313.82	258.41	64.23	68.48	181.35
Colon	254.16	199.14	122.32	120.21	177.02
Lumbar spine	125.53	155.10	148.10	146.52	143.02
Muscle	88.09	100.89	158.21	159.25	125.21
Skin	46.51	50.68	42.28	39.69	44.81
Testes	30.31	37.34	25.13	24.55	29.33
Eye lenses	13.07	9.39	26.63	11.88	15.08
Cranium	8.87	15.96	23.79	13.01	15.06
Brain	8.52	16.51	23.68	12.87	15.03
Anklea and foot bones	8.63	15.94	23.93	12.16	14.81
Mandible	12.22	6.90	20.26	13.47	13.15
Salivary glands	11.57	13.77	18.48	11.90	13.79
Kidney	8.33	8.94	11.58	11.36	9.99
Tibia, fibulae, and patellae	5.88	11.01	12.97	7.63	9.18
Cervical spine	7.71	10.23	10.38	7.30	8.83
Pancreas	7.96	9.25	8.18	8.34	8.41
Gall bladder	5.72	7.11	6.17	6.36	6.31
Adrenals	5.04	5.44	5.91	6.19	5.62
Stomach	4.65	5.07	4.32	5.04	4.77
Liver	4.21	4.45	4.87	4.65	4.53
Clavicles	3.40	2.03	5.17	5.36	3.98
Spleen	3.11	3.37	4.27	5.11	3.94
Scapulae	1.95	2.58	5.82	5.20	3.81
Ribs	3.03	3.11	3.96	4.05	3.52
Thyroid	4.30	1.86	2.38	2.78	2.90
Esophagus	3.23	2.42	2.50	3.13	2.84
Heart	2.76	2.23	2.39	2.97	2.60
Lungs	2.49	2.21	2.46	2.73	2.48
Sternum	3.29	1.61	2.09	2.40	2.39
Thymus	2.93	1.33	1.88	2.40	2.18

nodes, testes, and colon received high values of neutron equivalent dose in the AP irradiation. While liver received greater value of neutron equivalent dose in the RLAT and salivary glands received low values of dose in the PA.

Table 3 Neutron equivalent dose calculated for different organs/tissues (mSv/Gy). The relative uncertainties are included in parenthesis

Organ/tissue	AP	PA	RLAT	LLAT	Total
Prostate	0.21 (0.06)	0.16 (0.07)	0.05 (0.08)	0.06 (0.07)	0.12 (0.04)
Rectum	0.13 (0.07)	0.25 (0.08)	0.06 (0.09)	0.06 (0.09)	0.12 (0.05)
Sacrum	0.01 (0.05)	0.26 (0.04)	0.05 (0.06)	0.07 (0.06)	0.11 (0.03)
Urinary bladder	0.58 (0.05)	0.07 (0.07)	0.06 (0.08)	0.06 (0.07)	0.21 (0.04)
Pelvis	0.13 (0.03)	0.08 (0.03)	0.08 (0.04)	0.11 (0.03)	0.11 (0.02)
Lymphatic nodes	0.36 (0.03)	0.09 (0.04)	0.08 (0.04)	0.12 (0.03)	0.17 (0.02)
Femora	0.14 (0.03)	0.08 (0.03)	0.13 (0.03)	0.16 (0.03)	0.13 (0.02)
Small intestine	0.34 (0.03)	0.05 (0.04)	0.07 (0.05)	0.13 (0.04)	0.15 (0.02)
Colon	0.32 (0.03)	0.06 (0.04)	0.07 (0.05)	0.25 (0.04)	0.19 (0.02)
Lumbar spine	0.06 (0.05)	0.14 (0.06)	0.04 (0.06)	0.04 (0.05)	0.07 (0.03)
Muscle	0.22 (0.01)	0.23 (0.01)	0.22 (0.01)	0.27 (0.01)	0.23 (0.01)
Skin	0.07 (0.01)	0.07 (0.01)	0.08 (0.01)	0.08 (0.01)	0.07 (0.01)
Testes	0.7 (0.09)	0.05 (0.1)	0.05 (0.25)	0.06 (0.15)	0.23 (0.08)
Cranium	0.11 (0.05)	0.12 (0.05)	0.20 (0.04)	0.17 (0.04)	0.15 (0.02)
Brain	0.01 (0.06)	0.14 (0.06)	0.24 (0.05)	0.2 (0.06)	0.17 (0.03)
Ankles and foot bones	0.26 (0.04)	0.17 (0.05)	0.37 (0.04)	0.35 (0.04)	0.29 (0.03)
Mandible	0.25 (0.07)	0.03 (0.11)	0.21 (0.09)	0.25 (0.08)	0.2 (0.05)
Salivary glands	0.32 (0.08)	0.18 (0.12)	0.32 (0.1)	0.32 (0.09)	0.29 (0.05)
Kidneys	0.04 (0.06)	0.17 (0.06)	0.01 (0.08)	0.14 (0.06)	0.10 (0.03)
Tibiae, fibulae, and patellae	0.22 (0.03)	0.16 (0.03)	0.19 (0.04)	0.19 (0.04)	0.2 (0.02)
Cervical spine	0.11 (0.06)	0.07 (0.08)	0.04 (0.07)	0.05 (0.1)	0.07 (0.04)
Pancreas	0.12 (0.08)	0.05 (0.08)	0.03 (0.08)	0.06 (0.09)	0.07 (0.05)
Gall bladder	0.14 (0.08)	0.04 (0.11)	0.11 (0.09)	0.02 (0.1)	0.08 (0.05)
Adrenals	0.03 (0.1)	0.20 (0.1)	0.07 (0.09)	0.12 (0.14)	0.10 (0.06)
Stomach	0.20 (0.05)	0.05 (0.07)	0.02 (0.11)	0.21 (0.06)	0.12 (0.04)
Liver	0.15 (0.04)	0.07 (0.05)	0.21 (0.05)	0.03 (0.06)	0.11 (0.03)
Clavicles	0.22 (0.07)	0.03 (0.08)	0.04 (0.15)	0.05 (0.09)	0.1 (0.05)
Spleen	0.04 (0.1)	0.23 (0.09)	0.03 (0.15)	0.42 (0.07)	0.17 (0.05)
Scapulae	0.03 (0.05)	0.09 (0.04)	0.05 (0.045)	0.05 (0.05)	0.05 (0.02)
Ribs	0.09 (0.03)	0.12 (0.03)	0.12 (0.03)	0.14 (0.03)	0.12 (0.02)
Heart	0.15 (0.05)	0.06 (0.06)	0.04 (0.07)	0.01 (0.06)	0.09 (0.03)
Lungs	0.14 (0.04)	0.12 (0.04)	0.08 (0.05)	0.10 (0.04)	0.11 (0.02)
Sternum	0.44 (0.07)	0.03 (0.23)	0.04 (0.13)	0.05 (0.11)	0.15 (0.06)
Thymus	0.28 (0.12)	0.03 (0.09)	0.04 (0.14)	0.05 (0.16)	0.10 (0.09)
Cartilage	0.27 (0.06)	0.14 (0.05)	0.14 (0.05)	0.17 (0.06)	0.18 (0.03)
Residual tissue	0.35 (0.01)	0.3 (0.01)	0.3 (0.1)	0.37 (0.01)	0.34 (0.004)

The comparison between equivalent dose of neutrons and photons for some organs/tissue are shown in the Fig. 4. As it can be seen, despite of photon doses, the values of neutron equivalent doses did not vary in the large range and their deposited doses were in the same order of magnitude, approximately. For instance, the ratio of photon equivalent dose of pelvis (which was placed in the treatment area) to that of the brain (which was located out of the treatment area) was 213.8, while this ratio for neutron equivalent dose was 0.8. Although, there were huge differences between the photon equivalent doses of these two organs, there were no significant differences between the neutron equivalent doses received by them.

It is important to note that neutron equivalent doses were not very higher in the treatment area, and they did not decrease by increasing the distance from the target volume, so that they were nearly homogeneous compared to photon dose distributions. The reason of this behavior was that the neutrons produced in the jaws of linac's head, did not pass through the patient in a direct path, but they scattered from jaws, floor, and walls of treatment room and reached to the body. Therefore, the normal tissues located farther from the tumor volume, received unwanted dose from neutrons.

In the Table 4, the calculated neutron equivalent doses of some organs were compared with those calculated and measured by Howell for 15 MV linac [20]. They calculated
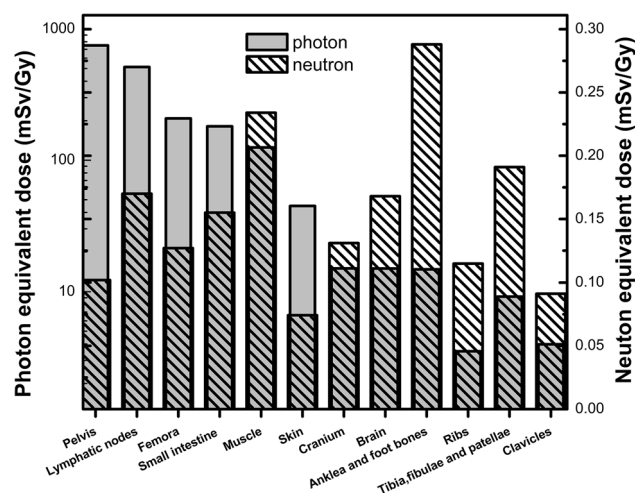
Fig. 4 Comparison between neutron and photon equivalent dose for some organs

Table 4 Comparison between the neutron equivalent dose values (mSv/Gy) calculated in this study and reported by Howell et al. (The relative uncertainties are included in parenthesis)

Organ	This work	By Howell et al.
Urinary bladder	0.21 (0.04)	0.2
Colon	0.19 (0.02)	0.13
Stomach	0.12 (0.04)	0.05
Liver	0.11 (0.03)	0.13

Table 5 Calculated fatal cancer risk due to photoneutrons for various organs in terms of a 70 Gy treatment dose

Organ	Calculated fatal cancer risk (%)
Active marrow	0.005
Bone surface	0.0005
Colon	0.01
Lung	0.007
Stomach	0.01
Bladder	0.004
Esophagus	0.001
Liver	0.001
Thyroid	0.0006
Skin	0.0001
Gonads	0.002
Remainder of body	0.004
Total	0.05

the neutron fluence at the position of organs, and the neutron equivalent dose using analytical function. The reported values were in order of magnitude of our values, but the differences may originate from the simplified process considered in their calculations. We simulated the patient body in details in the MCNP input and calculate the organs dose, while in their calculation the deposited mean value was not considered in the organ or tissue. However, the Monte Carlo calculations showed good agreements with measured data.

Neutron effective dose was also calculated using tissue weighting factors recommended by ICRP 103 and was obtained 0.2 ± 0.01 mSv/Gy. This value may appear small at first glance. Due to the high biological effect of neutrons on cancer induction, small neutron doses are also important. As some authors stated, in the radiotherapy with linac, neutron contamination delivers an undesirable dose in the patient that is less than 2.5 % of prescribed dose [6, 9, 10].

Risk assessment

Table 5 shows the calculated fatal secondary cancer risk values due to photoneutrons for various organs. Risk to breast was not considered, because this study analyzed

treatment for prostate cancer of male patient. To assess these risks, the total neutron equivalent doses (sum of the all orientation) were multiplied by the coefficients of Table 1 for 70 Gy treatment dose. The results indicated that colon and stomach have the maximum risk of secondary cancer risk of 0.01 %, while the total risk is 0.05 %.

It is worth to note that with reduction in the age of cancer incidence and the effect of undesirable neutron dose on increasing the risk of secondary cancers, considering these neutron doses are important. Therefore, the arrangements should be done to reduce the neutron dose as far as possible.

Conclusion

The dose of neutrons produced in the high-energy linac operating above 8 MeV is not considered in the treatment planning, while these particles have high biological effects on the body. In this work the unwanted neutron dose from high-energy linacs were studied. Using the MCNP code the treatment planning of prostate was simulated and doses of photon and neutron were calculated in the different organs/tissues of the patient-specific voxel phantom. As expected, the photon dose in the organs close to treatment area was higher than the doses of farther organs. Increasing the distance from the treatment area decreased the photon dose. However, the neutron dose distribution was almost homogenous in the whole body and was independent from the distance between organ and the irradiation area. This distribution caused an unwanted dose to be received in healthy tissues. Consequently, the risk of secondary cancer increases in normal tissues.

References

1. Chibani O, Ma CM (2003) Photonuclear dose calculations for high-energy photon beams from Siemens and Varian linacs. Med Phys 30:1990–2000
2. Sanchez-Doblado F, Domingo C, Gomez F, Sanchez-Nieto B, Muniz JL et al (2012) Estimation of neutron-equivalent dose in organs of patients undergoing radiotherapy by the use of a novel online digital detector. Phys Med Biol 57:6167–6191
3. Kry SF, Howell RM, Salehpour M, Followill DS (2009) Neutron spectra and dose equivalents calculated in tissue for high-energy radiation therapy. Med Phys 36:1244–1250
4. Vega-Carrillo HR, Hernandez-Almaraz B, Hernandez-Davila VM, Ortiz-Hernandez A (2010) Neutron spectrum and doses in a 18 MV LINAC. J Radioanal Nucl Chem 283:261–265
5. Vega-Carrillo HR, Ortiz-Hernandez A, Hernandez-Davila VM, Hernandez-Almaraz B, Montalvo TR (2010) H*(10) and neutron spectra around linacs. J Radioanal Nucl Chem 283:537–540
6. Vega-Carrillo HR, Baltazar-Raigosa A (2011) Photoneutron spectra around an 18 MV LINAC. J Radioanal Nucl Chem 287:323–327
7. ICRP (2008) The 2007 recommendations of the International Commission on Radiological Protection. ICRP 103, Pergamon
8. Ma A, Awotwi-Pratt J, Alghamdi A, Alfuraih A, Spyrou NM (2008) Monte Carlo study of photoneutron production in the Varian Clinac 2100C linac. J Radioanal Nucl Chem 276:119–123
9. Pena J, Franco L, Gomez F, Iglesias A, Pardo J, Pombar M (2005) Monte Carlo study of Siemens PRIMUS photoneutron production. Phys Med Biol 50:5921–5933
10. Difilippo F, Papiez L, Moskvin V, Peplow D, DesRosiers C, Johnson J, Timmerman R, Randall M, Lillie R (2003) Contamination dose from photoneutron processes in bodily tissues during therapeutic radiation delivery. Med Phys 30:2849–2854
11. Thalhofer JL, Rebello WF, Correa SA, Silva AX, Souza EM, Batista DV (2013) Calculation of dose in healthy organs, during radiotherapy 4-field box 3D conformal for prostate cancer, simulation of the Linac 2300, radiotherapy room and MAX phantom. Int J Med Phys Clin Eng Radiat Oncol 2:61–68
12. Martinez-Ovalle SA, Barquero R, Gomez-Ros JM, Lallena AM (2012) Neutron dosimetry in organs of an adult human phantom using linacs with multileaf collimator in radiotherapy treatments. Med Phys 39:2854–2866
13. Pelowitz DB (2008) MCNPX^{TM} user's manual. version 2.6.0. Los Alamos National Laboratory Report LA-CP-07-1473
14. ICRP (2009) Adult reference computational phantoms. ICRP 110, Pergamon
15. Hoseinian-Azghadi E, Rafat-Motavalli L, Miri-Hakimabad H (2014) Development of a 9-months pregnant hybrid phantom and its internal dosimetry for thyroid agents. J Radiat Res 55:730–747
16. Mohammadi N, Miri-Hakimabad H, Rafat-Motavalli L, Akbari F, Abdollahi S (2014) Neutron spectrometry and determination of neutron contamination around the 15 MV LINAC. J Radioanal Nucl Chem (under review)
17. Math Resolutions, LLC (2006) A program for radiation therapy treatment planning Columbia, Maryland 21045
18. NCRP (1993) National Council on Radiation Protection and Measurements. Limitation of exposure to ionizing radiation Report 116. Bethesda, MD
19. Martinez-Ovalle SA, Barquero R, Gomez-Ros JM, Lallena AM (2011) Neutron dose equivalent and neutron spectra in tissue for clinical linacs operating at 15, 18 and 20 MV. Radiat Prot Dosim 147:498–511
20. Howell RM, Hertel NE, Wang Z, Hutchinson J, Fullerton GD (2006) Calculation of effective dose from measurements of secondary neutron spectra and scattered photon dose from dynamic MLC IMRT for 6MV, 15MV, and 18MV beam energies. Med Phys 33:360–368